

Integrating Fiber Optic Strain Sensors into Metal Using Ultrasonic Additive Manufacturing

ADAM HEHR^{1,4}, MARK NORFOLK,¹ JUSTIN WENNING,¹
JOHN SHERIDAN,² PAUL LESER,³ PATRICK LESER,³
and JOHN A. NEWMAN³

1.—Fabrisonic LLC, Columbus, OH 43221, USA. 2.—Sheridan Solutions LLC, Saline, MI 48176, USA.
3.—NASA Langley Research Center, Hampton, VA 23681, USA. 4.—e-mail: ahehr@fabrisonic.com

Ultrasonic additive manufacturing, a rather new three-dimensional (3D) printing technology, uses ultrasonic energy to produce metallurgical bonds between layers of metal foils near room temperature. This low temperature attribute of the process enables integration of temperature sensitive components, such as fiber optic strain sensors, directly into metal structures. This may be an enabling technology for Digital Twin applications, i.e., virtual model interaction and feedback with live load data. This study evaluates the consolidation quality, interface robustness, and load sensing limits of commercially available fiber optic strain sensors embedded into aluminum alloy 6061. Lastly, an outlook on the technology and its applications is described.

INTRODUCTION

Real-time monitoring of engineering systems is improving speed, efficiency, and safety through enhanced operational decision making. Recently, real-time physical system monitoring has been combined with a virtual mathematical model of the system to increase decision making quality even further. This combined physical–virtual monitoring concept conceived within the US Air Force, called Digital Twin, feeds real-time information from the engineering system into its virtual “twin” or mathematical model in a control loop like framework for operation decision making and outcome prediction.^{1–3} Combination of the physical and virtual domains in the same framework reduces the need for overdesign (safety factors), enhances reliability, improves maintenance decisions, and revolutionizes safety. The Digital Twin approach is gaining traction quickly in the industrial sector as well through new products and designs.^{4,5}

A key component of the Digital Twin paradigm is its physical sensors and sensor systems for monitoring and feedback to the virtual twin. Historically, such health monitoring concepts have been difficult to implement because of the cost, high channel counts, data processing needs, computational power and memory, and sensors not measuring key events,

i.e., the sensor robustness and placement are not adequate to measure the state of concern.⁶ Consequently, state awareness or health monitoring systems that reduce the data quantity, simplify processing, and are robust in design are enabling large-scale health monitoring. Fiber optic strain sensors or fiber Bragg gratings (FBGs) fall into this enabling sensor category.

FBGs are miniature in size, made of glass, can be multiplexed, are immune to electromagnetic radiation, and are interrogated remotely. They have been successfully embedded in polymeric composites to measure unseen strain and damage states.^{6,7} The small size of the cable makes it minimally invasive to the structure, i.e., it does not influence or degrade material properties. Utilizing FBGs with metallic structures has been limited to external mounting until only recently with the advent of 3D printing. Even now, the high formation temperature of melt-based 3D metal printing technologies prohibits reliable FBG integration. Instead, the sensors crack from residual thermal stress.⁸ Ultrasonic additive manufacturing (UAM), a low temperature 3D metal printing technology, overcomes these formation challenges and has successfully been used to build FBGs into metal components for monitoring purposes.^{9,10} The incorporation of these sensors into the structure allows load states to be measured real-

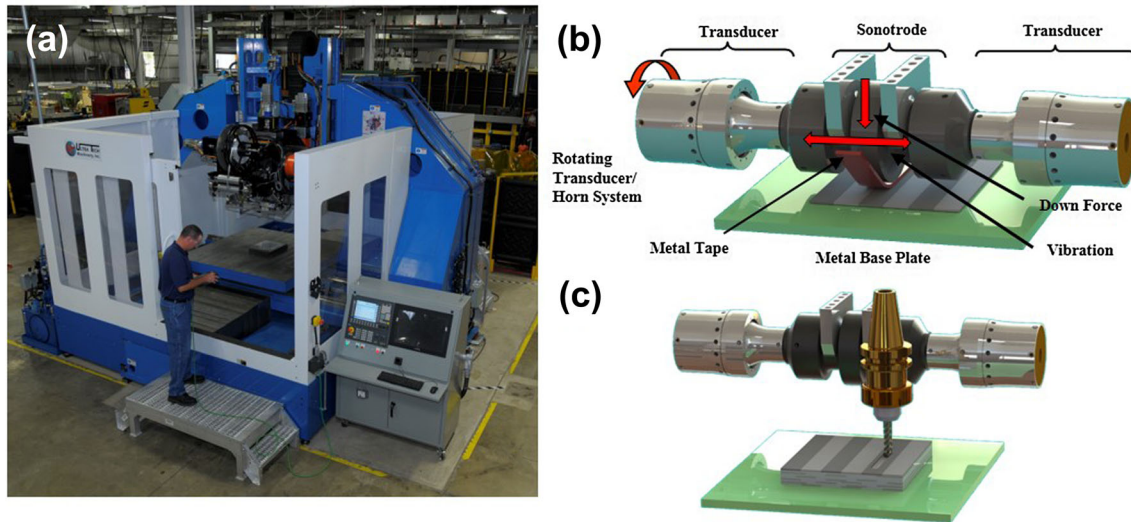


Fig. 1. UAM process: (a) Fabrisonic SonicLayer™ 7200; (b) additive or ultrasonic welding stage of the process; (c) subtractive or machining stage of the process. Reproduced with permission.¹⁵

time in localized regions, which in turn allows a reduction of the engineering safety factor and, ultimately, weight of the component.

The UAM process involves building up a solid metal part by ultrasonically welding a succession of metal tapes. Periodic machining operations are used interchangeably with the ultrasonic welding stage to introduce internal features and to finalize the geometry of the part.¹¹ Ultrasonic metal welding works by scrubbing metals together and not melting.¹² This scrubbing action generates heat on a localized level near the interface—approximately 150°C for aluminum and copper alloys.¹³ Because melting is not the mechanism for joining, controlled atmospheres are not required for the process and solidification microstructures are absent. These attributes enable technology scale-up for large parts with predictable properties, respectively.

A commercial UAM system is shown in Fig. 1a, while the additive and subtractive stages are shown in Fig. 1b and c, respectively. This UAM system has a build envelope near 2 m × 2 m × 1 m. The control variables for the additive stage are welder scrubbing amplitude (given typically in peak-to-peak amplitude), down force, translational travel speed, and an optional anvil pre-heat temperature. These control variables are shown in Fig. 1b. The scrubbing action is created by two high power ultrasonic transducers actuating the weld tooling, commonly called the sonotrode. The two transducers are operating in a push-pull configuration to enhance the energy delivery during the process.¹⁴

The solid-state, or no melting, nature of UAM enables integrating temperature sensitive components into the metal structure directly without damage, i.e., sensors. Further, the subtractive stage of the process allows accurate sensor placement within the structure during construction. As a result, metallic materials with localized sensor

placement now become possible. The goal of this study is to understand the embedding behavior of FBG sensors with Ormocer coatings and to benchmark the strain sensing limits of these embedded strain sensors through ASTM tensile testing. Finally, an outlook on the technology is described through examples of structures with embedded FBGs for NASA's Digital Twin program.

SAMPLE CONSTRUCTION

Ormocer® coated FBGs were obtained from FBGS* for this research. Ormocer®, short for organic modified ceramic, is a stiff plastic coating that enables strain transfer to the glass between -180°C and 200°C.¹⁶ With this coating, the fiber diameter is approximately 195 μm. The fiber optic cables used in this research have five gratings or independent sensors physically spaced 20 mm apart. The grating length itself is approximately 10 mm.

Prior to embedding the optical fiber, a slightly oversized channel is cut to enable location placement and to avoid sensor damage. The channel was cut using a 0.25 mm four-flute ball nose end mill to a 0.23 mm depth. The fiber was then placed into the cut channel and welded over with five layers of AA 6061 H18 foil. The foil thickness used to consolidate the fiber is 0.15 mm. The welding parameters used for encapsulation are a scrubbing amplitude of 32 μm peak to peak, a downforce of 4000 N, a translation speed of 4.44 m/min, and an ambient control temperature of 37.8°C. These welding parameters were selected from earlier pilot trials that demonstrated good consolidation quality around the fiber without damage to the fiber itself.

*<http://www.fbgs.com/>.

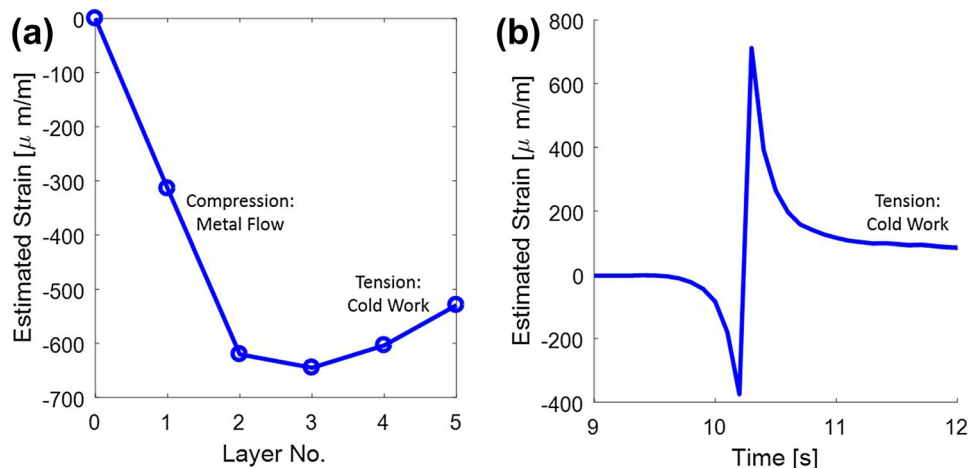


Fig. 2. Strain behavior during sample construction: (a) strain accumulation as a function of welded layers; (b) dynamic strain during welding for the fifth layer (zoomed in for visibility). The first layers of welding impart a compressive strain on the fibers, believed to be linked to the metal flow around the fiber. On the other hand, later layers accumulate tensile cold work from the rolling action of the welder.

These pilot trials confirmed a wide processing window, so parameters between extremes were selected in this study.

The strain or wavelength shift on the fiber during sample construction was measured to better understand consolidation behavior. FBG wavelength shift was recorded using a National Instruments PXIe system with a PXIe-4844 FBG card. Estimated strain response during construction was calculated using the literature gauge factor value, 0.78, for 1550-nm gratings.¹⁷ The representative in situ strain for one of the embedded FBGs is plotted in Fig. 2. The residual strain per layer is shown in Fig. 2a, while the instantaneous strain during the welding of layer 5 is shown in Fig. 2b. For the first few layers, the sensor enters a compression state. The sensor then begins to measure a reduction in the compressive strain with additional layers. It is suspected that the initial compression state occurs from the sensor getting squeezed during consolidation. The squeezing action may occur from the plastic flow of metal around the sensor. Plastic flow around embedded fiber-like materials has been observed before in UAM and the microstructures have been studied.^{18–21} After the second layer, the compressive state begins to decrease because the rolling action of the welder generates plastic strain within the part. The evolution of this cold work plastic strain is not well understood after layer 5 and requires further study, i.e., to identify if or when cold work ceases.

After layer addition, the subtractive stage of the UAM process was used to cut out ASTM tensile samples; see Fig. 3a. An exterior strain gauge was then added to the tensile sample for future comparative strain measurements and calibration. A representative cross-section of an embedded Ormocer[®] coated fiber is shown in Fig. 3b. The fiber is completely consolidated, which enables reliable strain transfer to the glass fiber.

TESTING AND CALIBRATION

Three tensile samples were manufactured and tested in this study using the same materials and procedures. Further, each sample has five gratings or sensors, enabling study of 15 data points. A single data trace is shown in this study, which is representative of the total sample behavior.

To evaluate strain-sensing limits as a function of load and for calibration purposes, cyclic tensile testing was carried out using a hydraulic load frame. This testing was done at various stress levels using a 0.5 Hz sinusoidal waveform. Force and displacement were measured in addition to foil gauge and FBG strains. The same PXIe system was used to measure the optical wavelength in this experiment. Foil gauge strain was measured using a PXIe-4330 strain card. The force and displacement were measured by recording calibrated voltage outputs using a PXI-4462 voltage card. All measured waveforms were synchronized to the same sampling clock.

Correlated foil gauge strain and normalized FBG wavelength shift are shown in Fig. 4a for a load level near half the ultimate tensile strength of AA 6061-T6 (157 MPa). The two quantities track each other well qualitatively and do not demonstrate any noticeable divergence. The calibrated sensor gauge factors were found to be consistent at different stress levels. The calculated gauge factor values ranged between 0.705 and 0.72, which is less than 10% difference when compared to the published literature value of 0.78. These gauge factors were calculated using linear regression for a first order polynomial (straight line fit).

This tensile sample design creates a uniform axial strain field when stretched since the sample is solely loaded in this direction. This axial strain field is equal on the outside and inside of the part. This strain equality is confirmed during testing because of the small error between the measured and

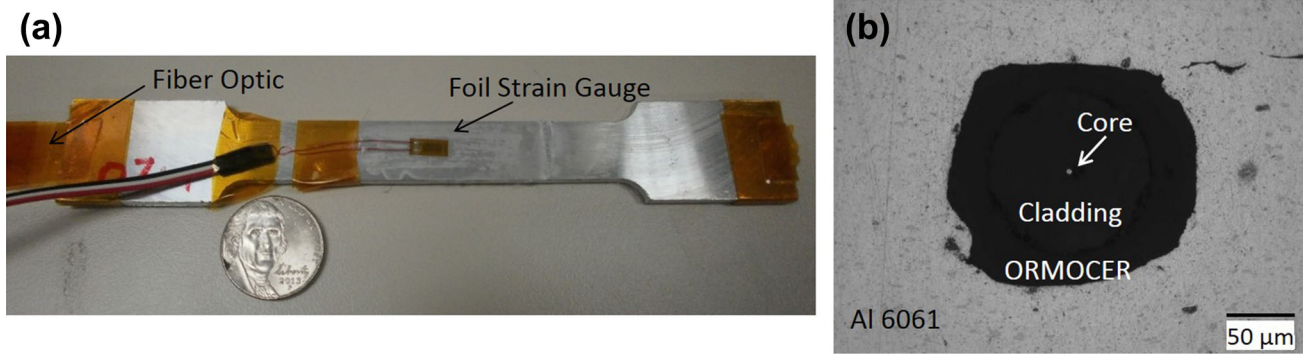


Fig. 3. Embedded fiber optic strain sensors: (a) ASTM tensile sample used to evaluate strain sensing performance; (b) micrograph of representative consolidated fiber showing metal completely encapsulating the fiber.

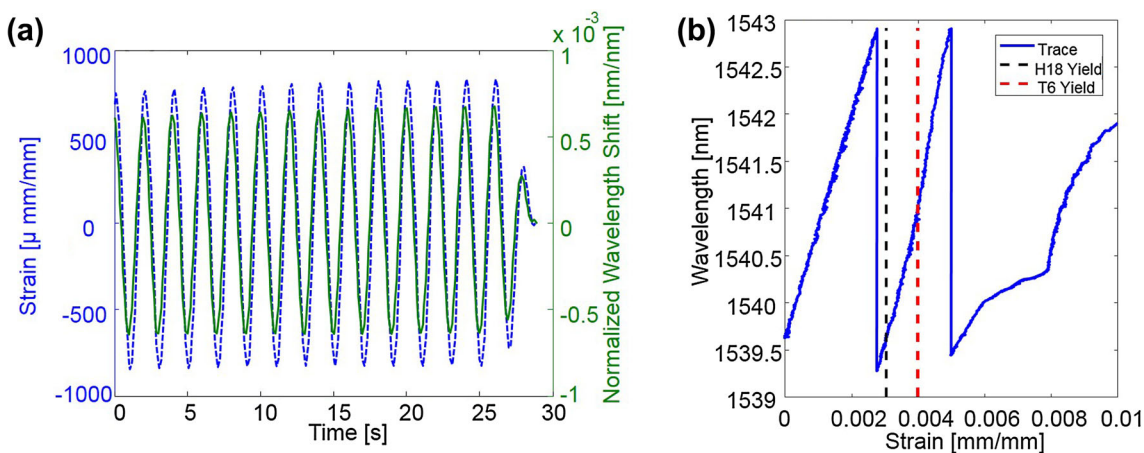


Fig. 4. Tensile testing: (a) exterior strain and embedded FBG wavelength shift (not calibrated strain) cyclic profile comparison; (b) wavelength response versus strain during strain limit testing. In (b), the embedded FBG tracks past the yield limit of the weld (H18) and baseplate (T6) materials. A sawtooth pattern is seen because the strain exceeds the set wavelength bounds in the interrogator for a given FBG as the sample is stretched. As a result, the strain from multiple FBGs is seen in the graph.

theoretical gauge factors for the FBG. Poisson ratio effects create a lateral strain field in the sample and ultimately a compressive stress or interface strain because the materials have different Poisson ratios. The sensor will not measure this interface strain because the fiber and aluminum have a fixed constraint in the axial direction (if perfect bonding is assumed). In practice, the external strain state may not be as easy to correlate to the internal strain state because of the presence of multi-axis loading and bending effects. In this case, sophisticated finite element models may be required to correlate the external and internal strain.

Strain-to-failure testing was used to evaluate the strain sensing limit of the embedded FBG; see Fig. 4b. The FBG and foil gauge exhibit linear correlation past the weld and baseplate material yield points and diverge with the onset of plasticity in the sample. A sawtooth pattern is observed because the wavelength shift exceeds the set wavelength bounds in the interrogator—simply a signal-processing limitation. Consequently, multiple sensors pass through a given wavelength band during testing.

Some of the tested samples (not shown) demonstrated intermittent fiber pull-out after the aluminum broke. The fiber broke simultaneously with the aluminum in others. This failure region was outside the sensing limits of the interrogator.

SUMMARY AND TECHNOLOGY OUTLOOK

UAM was used to embed fiber optic FBG strain sensors into aluminum ASTM tensile samples. Concurrent with sample manufacture, the fiber strain was measured. The first few consolidation layers create a large compressive stress, while later layers relieve some of this compressive stress through the consecutive rolling action of the welder. After the samples were built, quasi-static and cyclic tensile testing was used to evaluate strain sensing performance. The embedded sensors do not demonstrate slip behavior until after the yield point of the material and their calibration is close to the literature values.

This fundamental work enabled the creation of more complicated structures for evaluation. Recently, the team built a fatigue specimen

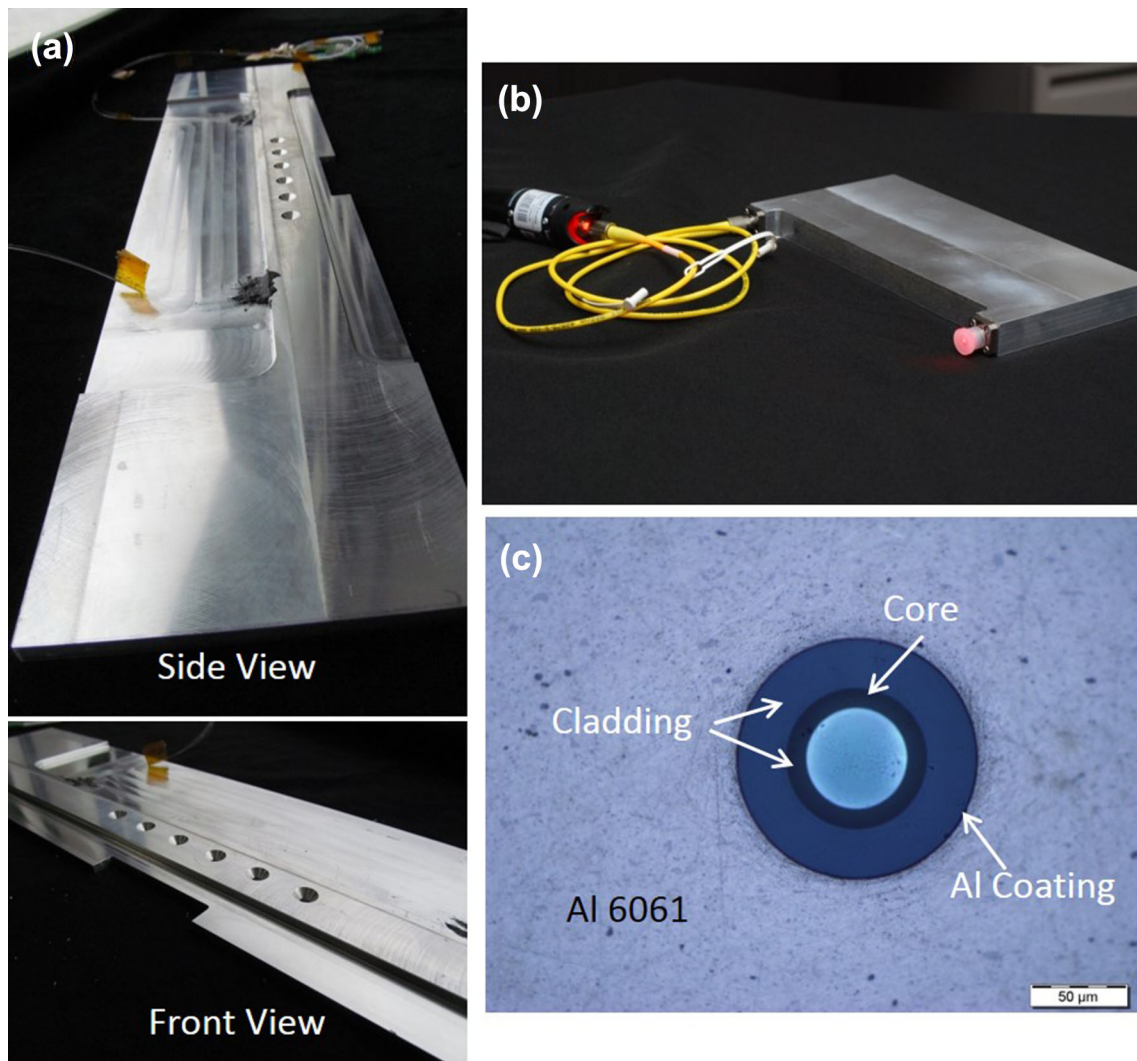


Fig. 5. Outlook on technology: (a) fatigue specimen developed by NASA's Digital Twin Project with 30 embedded FBG sensors near the stress concentrators in the sample (see bolt holes and notch in front view); (b) embedded FBG connector for robustness; (c) metallized fiber optic cables to expand the useable temperature range.

designed by NASA's Digital Twin program; see Fig. 5a. The specimen is designed such that failure is difficult to predict. This fatigue specimen is approximately 10 cm × 51 cm in size, exhibits complex geometry, and has 30 FBG sensors located around stress concentrators within the part. The team is also working toward enhancing the robustness of the embedded fiber optic systems (see Fig. 5b) and using metallized coatings to expand the temperature operation regime (see Fig. 5c). Flight hardware is also being developed with embedded sensors near critical stress points within the parts.

ACKNOWLEDGEMENTS

The authors acknowledge financial support from NASA's SBIR Office, NNX16CL33C. The authors are grateful for the support of NASA's Convergent Aeronautics Solutions (CAS) Program Digital Twin Project.

REFERENCES

1. E. Tuegel, A. Ingrassia, T. Eason, and S. Spottswood, *Int. J. Aerosp. Eng.* 2011 (2011). <https://doi.org/10.1155/2011/154798>.
2. G.W. Hunter, D.E. Berger, J.D. Lekki, R.W. Mah, D.F. Perey, S.R. Schuet, D.L. Simon, and S.W. Smith, Report No. 217825, NASA, Cleveland, OH, March 2013.
3. E.H. Glaessgen and D. Stargel, in *Proceedings—AIAA/ASME/SAE Structures, Structural Dynamics and Materials Conference* (2012).
4. C.J. Parris, J. Laflen, M. Grabb, and D. Kalitan, The future for industrial services: the Digital Twin, <https://www.infosys.com/insights/digital-future/Pages/future-industrial-digital.aspx>. Accessed 22 Aug 2017.
5. Siemens, The Digital Twin, <https://www.siemens.com/customer-magazine/en/home/industry.html>. Accessed 2 Oct 2017.
6. D. Huston, *Structural Sensing, Health Monitoring, and Performance Evaluation*, 1st ed. (Boca Raton: CRC Press, 2011), pp. 5–15.
7. K. Kuang and W. Cantwell, *Appl. Mech. Rev.* 56, 493 (2003).

8. D. Havermann, J. Mathew, W.N. MacPherson, D.P. Hand, and R.R. Maier, in *Proceedings of the SPIE* (2015).
9. C. Mou, P. Saffari, D. Li, K. Zhou, L. Zhang, R. Soar, and I. Bennion, *Meas. Sci. Technol.* 20 (2009). <http://iopscience.iop.org/article/10.1088/0957-0233/20/3/034013/meta>.
10. J. Schomer, A. Hehr, and M. Dapino, in *Proceedings of the SPIE* (2016).
11. D. White, *Adv. Mater. Process.* 161, 64 (2003).
12. K. Graff, J. Devine, J. Keltos, N. Zhou, and W. Roth, in *AWS Welding Handbook* (2001), p. 263.
13. M. Sriraman, M. Gonser, H. Fujii, S. Babu, and M. Bloss, *J. Mater. Process. Technol.* 211, 1650 (2011).
14. K. Graff, M. Short, and M. Norfolk, in *Solid Freeform Fabrication Symposium Proceedings* (2010).
15. A. Hehr, J. Wenning, K. Terrani, S.S. Babu, and M. Norfolk, *JOM* 69, 485 (2017).
16. FBGS, Ormocer coating, <http://www.fbgs.com/technology/why-we-have-chosen-to-use-an-ormocer-coating/>. Accessed 23 Aug 2017.
17. M. Kreuzer, Strain measurement with fiber Bragg grating sensors, <https://www.hbm.com/en/3189/tips-and-tricks-strain-measurement-with-fiber-bragg-grating-sensors/>. Accessed 2 Oct 2017.
18. C. Kong and R. Soar, *Appl. Opt.* 44, 6325 (2005).
19. D. Li and R. Soar, *J. Mater. Sci. Eng. A* 498, 421 (2008).
20. R. Friel and R. Harris, *Proc. Inst. Mech. Eng. Part L* 224, 31 (2010).
21. A. Hehr and M. Dapino, *Compos. Part B* 77, 199 (2015).